Real-time Recording of the Cellular Effects of the Anion Transporter Prodigiosin

Shane Cheung,[1] Dan Wu,[1] Harrison C. Daly,[1] Nathalie Busschaert,[2‡] Marina Morgunova,[1] Jeremy C. Simpson,[3] Dimitri Scholz,[3] Philip A. Gale,[4]* & Donal F. O'Shea[1,5]*

[1] Department of Pharmaceutical and Medicinal Chemistry, Royal College of Surgeons in Ireland, 123 St Stephen's Green, Dublin 2, Ireland.

[2] Chemistry, University of Southampton, Southampton, SO17 1BJ, UK.

[3] School of Biology and Environmental Science and Conway Institute of Biomolecular and Biomedical Research, University College Dublin, Belfield, Dublin 4, Ireland.

[4] School of Chemistry, University of Sydney, NSW 2006, Australia.

[‡] Current address: Department of Chemistry, Tulane University, New Orleans, Louisiana 70118, United States.

[5] Lead contact

*Correspondence: donalfoshea@rcsi.ie; philip.gale@sydney.edu.au

Summary

The unravelling of the cellular effects of anion transporters is key to their potential development as apoptosis inducing or autophagy disrupting therapeutics. A systematic study of the cellular responses to the anion transporter prodigiosin has been conducted using a pH *on/off* responsive NIR-fluorescent probe in HeLa and LAMP1-GFP transfected HeLa cell lines. The sequence of localized and global cellular acidity changes and resulting outcomes induced by the anion transporter have been visualized with high temporal and spatial resolution. The results show that prodigiosin causes the pH within the lysosomal lumen to rise following which, a non-organelle specific increase in acidity of the cytosol takes place which prompts cells to undergo apoptosis. This was confirmed by the quantification of NIR-emissive lysosomes, the intra-cellular fluorescence intensity and fluorescence volume over time. This NIR-probe overcomes the limitations of acridine orange which, to date, have severely restricted researchers in this field.

Introduction

Lipid membranes surrounding the cell and intracellular organelles perform numerous essential roles such as regulating the passage of biomolecules, maintaining ion gradients and controlling intracellular compartmental pH. Regulation of transmembrane ion transport into, out of, and within the cell is required to maintain ion homeostasis and the different ion concentrations within organelles essential for their normal function.[1] The maintenance of differing–intracellular ion concentrations and pH within subcellular regions is primarily achieved by cross membrane ion transport through specific channels and transporters.[2] Lysosomes are the most acidic cellular organelles with an intra-lysosomal pH of 4.5-5.0 (pH$_{lys}$) and are surrounded by the slightly above neutral cytosol, at pH 7.2 (pH$_{cyt}$) (Figure 1). Their primary cellular role is the degradation of materials compartmentalized within them by endocytosis, phagocytosis or autophagy.[3] Lysosomes contain numerous different hydrolases for these digestive roles and as such they must create and maintain a strongly acidic environment which is achieved by vacuolar-ATPase proton pumps embedded in their membranes. These pumps transport protons into the lysosomal lumen in an electrogenic process which generates a positive membrane potential inside the lysosome. Dissipation of positive charge is achieved by influx of anions such as Cl$^-$, through the transmembrane anion channel ClC-7 and further supported by efflux of cations such as K$^+$ (Figure 1).[4,5,6]

There is a growing interest in purposefully manipulating ion concentrations and pH within lysosomes in an effort to gain therapeutic benefit.[7,8] Several small molecule transporters, which modulate lysosomal and cytosolic ion concentrations and pH, have been shown to disrupt autophagy and induce apoptosis, leading to their recognition as potential antitumor pharmaceuticals.[9,10,11,12] Molecular anion transporters have been shown to cause a decrease in cellular cytosolic pH which can act as a trigger for a downstream release of pro-apoptotic proteins.[13,14] Recently, the first evidence of small molecule ion transporters capable of disrupting cell autophagy and inducing apoptosis has been disclosed.[6,9] As the levels of autophagy are generally higher in cancer than in normal cells, synthetic disruptors of cell autophagy offer potential as chemotherapeutic agents by depriving cancerous growths of nutrients derived from the recycling of cellular material.

One of the most widely studied small molecule anion transporters is the pigment prodigiosin, produced as a secondary metabolite by the *Serratia marcascens* strain of bacteria (Figure 2).[12,15,16]

Prodigiosin is one of a few known, non-peptide, natural products which can act as a chloride anion binder capable of transport across lipid bilayer membranes. It is amphiphilic in nature which facilitates its ability to insert into and/or cross membranes. The protonated form of prodigiosin binds to chloride through three hydrogen bonds formed with its methoxytripyrrole aromatic core which are further stabilized by electrostatic interactions (Figure 2).[17,18] Previous reports have described the anion transporting capabilities of prodigiosin and related synthetic anion transporters which have provided an essential basis for understanding the structural features that enable binding and transport of chloride ions.[19,20,21] In studies using model membrane systems and cancer cells, prodigiosin has been shown capable of acting as a H^+/Cl^- symporter.[22] Results from its screening against the US National Cancer Institute 60 human tumor cell lines have shown it to have broad spectrum cytotoxicity which has prompted extensive development of this compound class and other synthetic anion transporters towards clinically useful therapeutics.[23] For example, Obatoclax, a compound structurally related to prodigiosin, proceeded to phase II clinical trials for treatment of acute myeloid leukemia but was not developed further due to disappointing in-human efficacy and uncertainties surrounding its exact mode of action (Figure 2).[24] This highlights the continued importance of being able to accurately assess the cellular effects of small molecule anion transporters and gain a more in-depth understanding of their modes of action.

The cancer cell apoptosis inducing properties of prodigiosin and other related compounds have been shown to be closely associated with their anion transport properties and their ability to increase pH-$_{lys}$ and decrease pH-$_{cyt}$.[25,26,27] Such changes in acidity levels are known triggers for the downstream release of pro-apoptotic proteins such as cytochrome c and caspases from the mitochondria.[13,14]

In vitro fluorescence imaging of the effects of anion transporters and other lysosomal function disruptors in live cells offers an informative way of monitoring the ability of anion transporters to affect intracellular acidity levels and subsequent cellular responses. To date, this has been almost exclusively carried out using the metachromatic dye acridine orange (AO) as an acidic organelle stain (Figure 2).[11,21,26,28,29,30] AO has a green colored emission (480-540 nm) but upon concentration induced aggregation it undergoes a bathochromic shift to a red emission (590-660 nm).[31] In live cell imaging, AO becomes protonated and positively charged in acidic organelles which restricts its transport across membranes giving rise to an increased localized concentration within these organelles. Once the concentration is sufficiently high, emission wavelength then

shifts from green to red. Experimentally, the loss of red fluorescence from an acidic organelle (following cell treatment with an anion transporter) is interpreted as the raising of the pH within the vesicle, causing deprotonation and reduction of concentration of AO within the organelle due to removal of the charge impediment to active transport out of the vesicle. Due to the severe limitations of AO as a probe this can only be done at a single time point, typically hours after treatment with the anion transporter. Recently, the restrictions and pitfalls of using AO as a lysosomal stain have been outlined, including its lack of selectivity (also stains DNA and RNA), the highly concentration sensitive nature of its red emission, high phototoxicity and low photo-stability.[32] In fact, the light induced toxicity of AO is used as an assay method to intentionally inflict damage on lysosomal membranes which makes it suitability for imaging lysosomal change questionable.[33] Other commonly used lysosomal probes such as lysotracker red are also not usable for continuous image data acquisition as they rapidly photo-bleach under imaging conditions.[32] These limitations have to date restricted researchers when imaging lysosomal disruption to single time-points, which is insufficient for gaining a comprehensive overview of these dynamic biological process. As such an imperative need exists for lysosomal probes that can meet all the challenging criteria to allow prolonged image capture of the sequential events caused by the disruption of normal lysosomal function. Such a probe would be a valuable tool for the screening and development of new transporter based therapeutics and as a means of investigating the complex cellular responses induced by these agents.

Recently some of us reported a NIR fluorescent BF_2-azadipyrromethene (NIR-AZA) lysosomal probe 1 with several key advantages over other probes such as low energy spectral wavelengths (λ_{max} emission 707 nm), low toxicity and excellent photostability (Figure 3a).[34,35]

It differs significantly from typical basic nitrogen containing lysosomotropic stains with an off to on fluorescence switch controlled by conversion of a phenolate to phenol. Emission from the probe is selective for the lysosomes and as the off/on switching mechanism is reversible, it is capable of real-time continuous imaging of lysosomal trafficking in 3D or 4D over prolonged time periods without perturbing normal cellular function.[34] These positive features are good indicators that 1 would also be capable of imaging cell responses to agents that perturb the normal pH profile of the cell.

As prodigiosin is a well-recognized and important benchmark anion transporter and lysosomal

disruptor, it was chosen for this study. The exact mode or modes by which prodigiosin and other anion transporters induce apoptosis in cancer cells is/are complicated due to the numerous intracellular targets and the multiple subsequent downstream cellular pathways that can be activated as a result of disrupting ion and pH homeostasis. It is commonly accepted, however, that prodigiosin has the ability to increase lysosomal pH and in some cell lines decrease cytosolic pH, both of which are known factors that can initiate a cascade of cellular events leading to apoptosis. Under normal pH cellular conditions, probe **1** has been previously shown to be present throughout the cytoplasm, though only emissive from the low pH lysosomes.[34] As such, it was envisaged that on perturbing cell pH homeostasis, both increasing (turning off) and decreasing (turning on) pH would be observable in different cellular regions over time. The approach adopted for this investigation was to first pre-stain lysosomes as NIR-emissive with probe **1** such that it may be possible to observe the prodigiosin induced lysosomal de-acidification causing loss of their emission while acidification of the cytosol may be observable as a turn on of fluorescence (Figure 3b). It has been previously shown that changes in lysosomal and cytosolic pH in HeLa cervical cancer cells induced by tumor necrosis factor-α or staurosporine are closely associated with the induction of apoptosis, though the action of prodigiosin on this cell line has not been investigated.[36] The goal of this work was to illustrate how probe **1** is capable of capturing the sequence of prodigiosin induced acidity changes and apoptosis in HeLa cells as they occur in real-time within a single experiment.

Results and Discussion

Monitoring the effects of prodigiosin in synthetic liposomal models with 1

Prior to intra-cellular imaging with **1**, a study was first conducted using synthetic liposomal models to confirm that fluorescence intensity changes from responsive probe **1** could be used to monitor prodigiosin induced effects on intra-liposomal pH. To carry out the study, probe **1** was encapsulated in 7:3 POPC:cholesterol vesicles buffered to pH 3 following standard literature protocols.[37] Preliminary experiments had shown that cholesterol-containing vesicles were stable enough at this low pH to conduct transport assays (Figure S1). At this pH fluorescence at 720 nm from encapsulated **1** (excitation at 686 nm) was readily measurable using a standard spectrometer. Vesicles containing **1** were suspended in solutions with three different pairs of internal and external salt combinations (i) internal NaCl (489 mM) / external Na_2SO_4 (162 mM) (ii) internal NaCl (489

mM) / external NaCl (489 mM) and (iii) internal Na_2SO_4 (162 mM) / external Na_2SO_4 (162 mM) (Figure 4a). Experiments were carried out on each suspension type with and without the addition of aqueous NaOH 60 sec prior to the addition of prodigiosin or DMSO as a negative control. This addition of base created a pH gradient from intra-vesicular pH 3.0 to extra-vesicular pH 5.0 which would be expected to drive proton transport. The emission of encapsulated **1** at 720 nm was monitored over time with the data representing changes in intra-vesicular pH shown as F/F_0 versus time, where F is the fluorescence intensity from **1** at a given time and F_0 is its fluorescence intensity at the beginning of the experiment, prior to the addition of prodigiosin or negative control (Figure 4b, 4c). The results show that for suspension (i) addition of prodigiosin leads to a rapid decrease in F/F_0 in both the presence and absence of a pH gradient. This decrease in F/F_0 can be explained by the prodigiosin mediated transport of H^+ out of the vesicles, leading to an increase in internal pH and quenching of the fluorescence of **1**. The fact that the internal pH is raised both in the presence and absence of a pH gradient implies that the positive Cl^- gradient present in both cases, is sufficient to drive H^+/Cl^- symport by prodigiosin at low pH. To test this hypothesis, the experiment was repeated on solution (ii) without the presence of a Cl^- gradient by including NaCl both inside and outside the vesicle. Under these conditions it was seen that prodigiosin could only alter the internal pH of the vesicle when a pH gradient was present to drive HCl transport and without that gradient no change in F/F_0 was observed (Figure 4c).

It has previously been proposed that for prodigiosin to transport HCl across lipid bilayers, chloride needs to be present in order to mediate the transport and alter the internal pH.[19,25,38] Experiments conducted with solution (iii) using Na_2SO_4 instead of chloride as both the intra- and extra-vesicular salt showed no changes in F/F_0, confirming that prodigiosin is unable to alter pH of the internal vesicle solution in this situation, even in the presence of a pH gradient. This is consistent with the known high hydration energy of the doubly negatively charged sulfate anion,[39] making the transport of sulfate unfavorable. Overall, using probe **1** it was confirmed that prodigiosin is able to transport H^+ across the membrane in the presence of chloride but not in the absence of chloride, and in the absence of a pH gradient prodigiosin is able to transport H^+ provided that there is a favorable Cl^- gradient. Both these findings are in agreement with our previous observation that the H^+/Cl^- cotransport by prodigiosin is non-electrogenic and cannot be separated.[40] With confirmation that probe **1** could accurately predict the anion-transport properties of prodigiosin in model vesicle systems, its use for real-time visualization of cellular responses upon treatment with

prodigiosin was next attempted.

Live-cell imaging of the effects of prodigiosin on HeLa-LAMP1/GFP cells

Previously reported cell imaging experiments most commonly utilized AO as the staining agent which has restricted researchers to a single time point image typically acquired between 1 and 6 h post treatment with prodigiosin.[11,21,26,28,29,30,41] What has not been observable to date is the real-time sub-cellular regional changes of pH followed by the subsequent cellular effects in one continuous imaging sequence. For this study HeLa Kyoto cells and a HeLa cell line stably expressing the lysosomal associated membrane protein-1 (LAMP1) fused to green fluorescent protein (GFP) were used.[34,42] HeLa-LAMP1-GFP cells make it possible to simultaneously identify lysosome membranes using a green emission filter (494-557 nm) and probe **1** (in its on state) in the lysosomal lumen with a NIR filter (679-727 nm).[34]

To detect the influence of prodigiosin on pH_{lys} in the immediate time period following its addition to cells, experiments were performed using the LAMP1-GFP expressing HeLa cell line, imaging simultaneously in both the green and NIR channels. HeLa-LAMP1-GFP cells were first incubated with **1** for 2 hr to NIR-stain the lysosomes, and then moved to a widefield microscope surrounded by an incubator to maintain the temperature at 37°C and CO_2 at 5%, following which a field of view containing suitable cells was chosen. Cells were treated with prodigiosin (50 µM) and multi-channel (GFP and NIR filters) time-lapse images were acquired in a single focal plane for 5 min with 20 sec intervals between image acquisitions. Representative time-lapse images, in the NIR and GFP channels, were compiled into a montage as shown in Figure 5. Visual analysis of the movie shows that prior to addition of prodigiosin individual lysosomes are clearly visible moving through the cell. In the NIR channel (Figure 5a) lysosomes labelled with probe **1** are still abundant in the perinuclear region 1 min after the addition of prodigiosin and the emission is closely aligned with the GFP emission shown in Figure 5b. However, the number of lysosomes stained with **1** begins to visibly decrease between 3 and 4 min, yet the GFP staining pattern remains constant. Between 4 and 5 min the number of NIR-fluorescent lysosomes is significantly reduced, indicating that pH_{lys} has increased and probe **1** has switched from *on* to *off* (Movie S1). In contrast, the quantity of GFP labelled lysosomes remains relatively unchanged for this time period, although there is a decrease in intensity attributable to the low photo-stability of GFP (Figure 5b, Movie

S2). GFP imaging beyond this time point was not possible due to complete photo-bleaching of GFP. Composite images from the NIR and GFP fluorescence channels show lysosomal co-compartmentalization of **1** and LAMP1-GFP up to 2 min after treatment with prodigiosin, but by 5 min there is significantly less red/green associated together, showing that the lysosomes are still visible but they are no longer stained with probe **1** (Figure 5c, Movie S3). In the expanded cellular view of images taken at 1 min post prodigiosin treatment the compartmentalization of emission from **1** (red color) within the GFP emitting lysosome membrane (green color) can be clearly seen for individual vesicles. This contrasts with the 5 min time point image in which the GFP emission remains and the NIR emission of **1** is absent in many of the lysosomes (Figure 5d, 5e).

The full field of view for this experiment showed numerous cells undergoing the same response to prodigiosin as described above (Figure S2 and Movie S4). This is strong evidence that prodigiosin can effectively cause lysosomal de-acidification and does so without destroying the lysosome membrane itself. It also highlights the advantage of using the reversible *on/off* fluorescence properties of probe **1** for real-time imaging of this dynamic cellular event.

3D Live-cell imaging of prodigiosin induced changes in HeLa Kyoto cells

Our next goal was to continually capture images from the time point of treatment of cells with prodigiosin through to apoptosis within a single experiment. If successful, this would allow the capture of the sequence of increasing pH within lysosomes followed by the subsequent responses of the cell to this inflicted stress. Unlike **1** which has excellent photo-stability, the susceptibility of GFP to photo-bleaching precluded its use in such prolonged imaging experiments, so HeLa cells were used. Following pre-incubation of HeLa cells for 120 min with **1** to stain the lysosomes, a field of view containing suitable cells was selected using a widefield microscope surrounded by an incubator to maintain required temperature and atmosphere. Prodigiosin was administered to the cells and image data acquired, in a single focal plane, for 40 min with 20 sec intervals between images giving a total of 120 images. Representative time-lapse images from 0 - 35 min were compiled into a montage as shown in Figure 6 (Movie S5).

Visual analysis of the time lapse movie shows that before the addition of prodigiosin, individual lysosomes are clearly visible moving through the cytoplasm. From 1 to 15 min the number of labelled lysosomes (punctuate bright spots) can be seen to decrease, indicating that lysosomal pH

has increased and the emission from **1** has been switched *off*. After 20 min, considerably fewer individual lysosomes are visible within the cytoplasm yet a more general increase in fluorescence intensity begins to emerge. This plausibly can be attributed to a non-organelle specific rise in the cytosolic acidity levels. From 20 min onwards, a more distinct decrease in pH of the cytosol occurs with NIR emission brightening significantly. At 25 min a relatively strong fluorescence is present throughout the cell body (excluding the nucleus) indicating that the decrease in cytosolic pH has caused previously non-fluorescent **1** to turn *on* in response to this change. At this point the cell body can be seen to contract in size indicating the onset of apoptosis. From 25 to 35 min the cell continues to round up, and fluorescence intensity increases dramatically due to a combination of decreasing pH and reduced cell volume (Figure 6 and Movie S5). A decrease in cytosolic pH has been previously proposed to be closely associated with the onset of induced apoptosis in HeLa cells.[36]

Further analysis of the observed sequence of events captured in this experiment was carried out by examining the changes in the global fluorescence intensity over time for an enlarged field of view containing five cells (Figure 7, Figure S3 and Movie S6). Changes in intracellular fluorescence intensity were determined by selecting five cells within the field of view as regions of interest (ROI) from the full field of view for this experiment. Using ImageJ software, the fluorescence intensity (I_{flu}) in each ROI was measured at each data acquisition time point over the 40 min, and plots of I_{flu} versus time constructed for each ROI (Figure 7b). It should be noted that the individual cell shown in Figure 6 is included in this analysis and is the cell numbered 1 in the bottom right hand corner of the image. These plots show that the time course of fluorescence intensity changes for each cell followed the same trends. Analysis of the normalized I_{flu} profiles shows that fluorescence intensity decreases immediately after treating the cells with prodigiosin, and that minimum fluorescence occurs at approx. 15 min. This was followed by a steady increase in I_{flu} for the remaining duration of the time-lapse experiment. Maximum I_{flu} occurs at 40 min, at which point the cells have completely rounded up. These results show for the first time, in a continuous format, the sequence of prodigiosin induced cellular events starting from lysosomal de-acidification, followed by a decrease in cytosolic pH and ending in apoptotic cell death.

4D HeLa Kyoto live-cell imaging of responses to prodigiosin

To obtain optimal spatial and temporal resolution of the prodigiosin induced dynamic events taking place within the cell, 4D live cell imaging was next carried out. To generate a three-dimensional representation of the cell in real time, a z-stack of multiple focal planes through the cell is acquired repeatedly throughout the experiment. This continual recording of cellular 3D volume over a period of time is termed four-dimensional (4D) imaging as the sample is imaged in the x,y,z and time dimensions, from which a time-lapse video of the 3D cellular volume can be created. Continuous live-cell imaging in the z-axis provides a more comprehensive method to imaging biological events within the 3D cellular volume over time. This is particularly relevant for imaging mobile vesicles, such as lysosomes, that move in and out of a single focal plane over time, and for following the progress of other changes occurring in the cytoplasm.

As previously described, HeLa Kyoto cells were pre-incubated with probe **1** for 2 hr, and moved to a widefield microscope surrounded within an incubator. Cell images were acquired with a z-stack comprising 15 focal planes every 30 sec for 40 min which equates to 1,200 individual images taken during the course of an experiment, which is only possible with a highly photostable fluorophore such as **1**. Unfortunately, the photostability of GFP was not sufficient for these experiments and as such HeLa Kyoto cells were used. Prior to addition of prodigiosin, a z-stack sequence was acquired to confirm that the emission from **1** was present in lysosomes and that the cells showed no obvious signs of stress (Figure S4a,b). Immediately after treatment with prodigiosin, 3D imaging of the same field of view commenced and was continued for 40 min (Figure 8). The resulting 4D dataset was de-convolved and compiled into a time-lapse movie using Huygen deconvolution software (Movie S7). Representative images from this movie, at ten min intervals, are shown as a montage in Figure 8a with enlarged cell images taken before and 40 min after addition of prodigiosin shown in Figure S4a and S4c. This overall sequence of events was consistent with what was observed in the previous 3D imaging experiment in that, a rapid loss of NIR-fluorescence from individual lysosomes occurred over the first 10 min. From 10 to 30 min a more diffuse emission became visible throughout the cytoplasm, which was no longer confined within individual vesicles. Comparison of individual z-stack images taken before and 40 min after addition of prodigiosin shows that a drastic change in the distribution of intracellular fluorescence had taken place throughout the 3D volume of the cell (Figure S4b and S4d). The highly defined punctuated regions of fluorescence that are notable in all of the z-stack slices at the outset are no

longer visible in any part of the cell after 40 min, being replaced by a diffuse fluorescence throughout the cytoplasm.

A distinct advantage of acquiring imaging data for the entire 3D cellular volume is that the dataset is amenable to further analysis and quantification. Using the single cell shown in Figure 8a as a ROI, changes in its fluorescence profile over time were determined. Using ImageJ software, the change in number of lysosomes over time was quantified following treatment of the cells with prodigiosin (Figure 8b). A plot of the number of NIR-stained lysosomes within the cell volume versus time showed a dramatic reduction in their number in the first minutes immediately after treatment, and the count number remained low for the remainder of the experiment. Using the same dataset, the changes in total fluorescence intensity (I_{flu}) from within the cell over the 40 min time period were determined, also using ImageJ software (Figure 8c). A plot of I_{flu} versus time showed that fluorescence intensity decreased immediately after the addition of prodigiosin, reaching a minimum at 4-5 min which coincides with the lowest number of stained lysosomes detectable. Following this time point, the cellular fluorescence intensity began to steadily rise and continued to increase until 25 min post administration of prodigiosin, following which the intensity level plateaued. These results are consistent with the proposed sequence of events that first lysosomes are de-acidified by prodigiosin, followed next by an increase in cytosolic acidity which can promote cell death.

A further independent 4D imaging experiment with a larger number of cells within the field of view was carried out, with *z*-stacks acquired every 20 sec over a 30 min time period. The resulting 4D imaging dataset, which contained ten cells in the field of view, was deconvolved and analysed for changes in stained lysosome numbers, fluorescence intensity and the fluorescent cellular volume over time. Representative time points from the experiment are shown in Figure 9a and are consistent with the results described above (Movie S8). A plot of the number of lysosomes stained with **1** showed that they rapidly decreased at the outset of the experiment (Figure 9c). Soon thereafter, from 5 min onwards, the general fluorescence intensity from the diffuse cytosol staining increased steadily reaching a maximum at 20 min (Figure 9d). Interestingly, while all the cells in the field of view overall responded to prodigiosin in the same manner within the 30 min time frame of the experiment, some cells changed their fluorescence staining patterns faster than others.

Finally, a further analysis of changing subcellular fluorescence volume was applied utilizing the Surface Tool function in Imaris image processing software. This was done by first applying an intensity threshold to the first frame of the 4D dataset to parameterize a baseline level of intracellular fluorescence from **1** which differentiated from background noise. These parameters were then applied to each *z*-stack and time point in the 4D dataset to generate a surface model of cellular fluorescence from probe **1** over time which was compiled into a movie format (Movie S9). Generating a surface model of fluorescence over time graphically illustrates the trends of intra-cellular pH responses from a number of cells and can also be used to provide a semi-quantitative measurement of how the volume of the cell which is fluorescent changes over time. A montage of selected single time point images from this time-lapse representation are shown in Figure 9b. In this analysis again the punctuated fluorescence of individual lysosomes was visible predominantly in the perinuclear region immediately after the addition of prodigiosin (Fig 9b, 1 min). After 10 min the 3D surface map which represents regions of the cell which are fluorescent had enlarged significantly, however some regions within some cells remain dark, indicating that not all of the cytoplasm has yet become fluorescent. From 10 to 30 min the fluorescent cell volumes continue to grow until the entire cell body is mapped as being NIR-emissive. A plot of changes in fluorescent cell volume versus time for all cells in the field of view showed that it increased from 5 min onwards reaching a maximum at 25 min (Figure 9e). This increase is similar to that of I_{flu} over time (Figure 9d) but with an added layer of detail showing that some cells responded faster than others, and some regions of the cytoplasm within specific cells acidified earlier than others.

Conclusions

To conclude, we have demonstrated, for the first time, continuous imaging of the dynamic intracellular events induced by the H^+/Cl^- transporter prodigiosin. Using 3D and 4D live cell imaging, the sequence of localized and global cellular acidity changes and resulting outcomes can be visualized with high temporal and spatial resolution. A systematic study of the cellular responses to prodigiosin has been conducted using fluorescent probe **1** in HeLa cells, including LAMP1-GFP transfected HeLa cell line, in 3D and 4D and with analysis of the acquired image data. The results show that prodigiosin can rapidly cause the pH within the lysosomal lumen to rise, though the membrane of the lysosome does appear to remain intact. Following this event, a non-organelle specific increase in acidity of the cytosol takes place which can prompt cells to

undergo apoptosis. In each experiment carried out, the sequence of cellular events has followed the same order, in that first the lysosomes de-acidify and then a cytosol pH decrease occurs. This was confirmed by three independent analysis methods which quantified changes to the number of NIR-emissive lysosomes, the intra-cellular fluorescence intensity and the subcellular fluorescence volume over time. The key to the imaging success of these experiments lies in the reversibility of the *on/off* NIR-fluorescent switch of probe **1**, its exceptional photo-stability, and low energy wavelengths. These attributes allow it overcome all the limitations of acridine orange which has severely restricted researchers to date. It is anticipated that probe **1** could be utilized for unravelling the mechanistic complexities of other apoptosis promoters and assist in the development of apoptosis inducing or autophagy disrupting therapeutics. It has now become imperative that more target specific probes capable of continuous live cell imaging are developed to keep pace with the advancements in imaging hard and software. Such probes will allow researchers to move from picture images to movies which are richer in data, allowing for more informed scientific interpretations of complex and interrelated biological events.

Experimental Procedures

All commercially available solvents and reagents were used as supplied, unless otherwise stated. Cholesterol was supplied by Sigma-Aldrich. POPC (1-palmitoyl-2-oleoyl-*sn*-glycero-3-phosphocholine) was supplied by Genzyme and was stored at -20°C as a solution in chloroform (1 g POPC in 35 mL chloroform). Octaethylene glycol monododecyl ether was used as detergent supplied by TCI. HeLa Kyoto cells purchased from ATCC. iDMEM media and geneticim purchased from Sigma. Prodigiosin was dissolved in DMSO sonicated for 5 min and diluted in PBS to make stock solution with a final concentration of 1.8 mM. Live-cell imaging done with 8 well glass bottomed slides from Ibidi consisted of eight independent wells on glass with a No. 1.5H (170 +/- 5 μm) thickness. Vectashield coverslip mounting media purchased from Vectorlabs. Phenol red-free imaging DMEM medium was used for all experiments. Absorbance spectra were recorded with a Varian Cary 50 Scan ultraviolet–visible spectrometer. Fluorescence spectra were recorded with a Varian Cary Eclipse Fluorescence Spectrometer. Solvents for absorbance and fluorescence experiments were of HPLC quality. Origin, SigmaPlot, ChemDraw, Zeiss LSM and ImageJ, Imaris, and Huygens software were used for data analysis.

Synthesis of unilamellar vesicles. A lipid film of 7:3 POPC:cholesterol was formed from a chloroform solution under reduced pressure and dried under vacuum for at least 4 hr. The lipid film was rehydrated by vortexing with the internal solution. The lipid suspension was then subjected to nine freeze-thaw cycles, where the suspension was alternatingly allowed to freeze in a liquid nitrogen bath, followed by thawing in a water bath. The lipid suspension was allowed to age for 30 min at room temperature and was subsequently extruded 25 times through a 200 nm polycarbonate membrane (Nucleopore^{TM}) using a LiposoFast-Basic extruder set (Avestin, Inc). The resulting unilamellar vesicles were dialyzed (Spectra/Por® 2 Membrane MWCO 12-14 kD) against the external medium to remove non-encapsulated salts. Internal and external solutions vary from experiment to experiment, but in general an ionic strength of 500 mM was used.

Confirmation of vesicle stability. POPC vesicles can be unstable at lower pH, but are stabilized by cholesterol and sulfate anions. In order to confirm that the vesicles used in this study are stable enough, a series of chloride selective electrode experiments were conducted. In brief, unilamellar 7:3 POPC:cholesterol vesicles containing NaCl (489 mM) buffered to pH 3.0 using a 5 mM citrate buffer were prepared as described above and were suspended in a Na_2SO_4 solution (162 mM) buffered to pH 3.0 using a 5 mM citrate buffer. A DMSO solution of either prodigiosin or **1** was added to start the experiment and the external chloride concentration was monitored using a chloride selective electrode. After 5 min detergent was added to calibrate the system to 100% chloride release (Figure S1a). In some cases, NaOH was added one min before the experiment in order to achieve a pH gradient across the membrane (pH 3.0 inside the vesicle and pH 5.0 outside) (Figure S1b). The results shown in Figure S1 show that neither prodigiosin nor **1** induce significant leakage of chloride anions under these conditions (HCl symport implies only small amounts of chloride transport that cannot be detected by the electrode). Furthermore, over the course of the experiment the values prior to the addition of detergent did not change significantly, indicating that 7:3 POPC:cholesterol vesicles are stable at pH 3.0 for at least four hr. In conclusion, this experiment has shown that the liposomes are stable and can be used in fluorescence tests for H$^+$ transport. Additionally, this experiment also showed that **1** itself does not disturb the liposomes itself and can be used as a silent monitor of intra-vesicular pH.

Monitoring of intra-vesicular pH changes with probe 1. Prior to carrying out the study, tests were carried out which confirmed that prodigiosin does not interfere with the fluorescence of **1**. The optimal settings for studying pH changes inside POPC:cholesterol vesicles were determined

as 686 nm for excitation and 720 nm for emission wavelength. The addition of detergent does not give any information regarding the end point of the transport process due to the large effect of the detergent on the fluorescence of **1**. For HCl symport assays, a lipid film of 7:3 POPC:cholesterol was formed from a chloroform solution under reduced pressure and dried under vacuum for at least 6 hr. The lipid film was rehydrated by vortexing with the internal solution (containing 489 mM NaCl or 162 mM Na_2SO_4 and 135 µM fluorophore **1**, buffered to pH 3.0 using a 5 mM citrate buffer). The lipid suspension was then subjected to nine freeze-thaw cycles and allowed to age for 30 min at room temperature before extruding 25 times through a 200 nm polycarbonate membrane. The majority of unincorporated dye and salts were removed by an overnight dialysis against the external medium (Spectra/Por® *2* Membrane MWCO 12-14 kD), followed by size exclusion chromatography on a Sephadex G-25 column using the external solution as eluent. Not all of **1** could be removed from the external solution by dialysis and size exclusion chromatography, though the remaining external fluorophore did not impede subsequent experiments. The thus obtained POPC:cholesterol vesicles containing **1** were suspended in the external medium with three different pairs of internal and external salt combinations (i) internal NaCl (489 mM) / external Na_2SO_4 (162 mM) (ii) internal NaCl (489 mM) / external NaCl (489 mM) and (iii) internal Na_2SO_4 (162 mM) / external Na_2SO_4 (162 mM). The lipid concentration per sample was 1 mM. The fluorescence intensity of encapsulated fluorophore **1** at 720 nm was monitored over time by excitation at 686 nm. A small amount of a DMSO solution of prodigiosin was added to initiate H^+ transport (neat DMSO was used as a negative control). In some cases, a small amount of NaOH was added 1 min prior to the addition of prodigiosin or DMSO in order to create a pH gradient of pH 3.0/pH 5.0 and drive H^+ transport (the pH gradient of pH 3.0 inside and pH 5.0 outside the vesicle was chosen based on the fact that the pK_a of **1** = 4 in DMEM).[34] Data is represented as F/F_0 versus time, where F is the fluorescence intensity at a given time and F_0 is the fluorescence intensity at the beginning of the experiment (after the addition of NaOH and prior to the addition of prodigiosin or DMSO). This way only the changes in internal pH are represented by the graphs. At the end of the experiment, the vesicles were lysed with 30 µL of octaethylene glycol monododecyl ether (0.232 mM in 7:1 water:DMSO v/v).

Live-Cell Imaging. Live-cell imaging was performed on a Zeiss AxioVert 200M epi-fluorescent widefield microscope equipped with an Andor iXon 885 EMCCD and controlled by Axiovision 2.0 software. Illumination was provided by a CoolLED pE-2 solid-state LED system

capable of excitation at 488 and 635 nm. Images were acquired with a Zeiss Plan-Apochromat 100 x/1.40 Oil DIC or Olympus ApoN 60x/1.42 Oil objective. The microscope was surrounded by an incubation chamber that allowed the temperature and CO_2 to be maintained at 37ºC and 5% respectively.

HeLa Kyoto or HeLa-LAMP1/GFP cells were seeded at a density of 1 x 10^4 cells/well on a glass bottomed chamber slide (Ibidi) and allowed to proliferate in the appropriate medium for 24 hr at 5% CO_2 and 37°C. Cells were incubated with **1** (1 x 10^5 M) for 120 min to label lysosomes. The slide was moved to the microscope stage, and a field of view with a suitable group of cells was selected using the NIR channel. An aliquot of prodigiosin stock solution (10 or 20 µL) was added to the well followed by the immediate acquisition of a time-lapse in a single focal plane, or 4D imaging acquiring z-stacks at each time-point. Z-stack = 15 focal planes over 17.15 µm. NIR **1**: excitation = 635 nm, emission filter = 649 nm (long pass). GFP: excitation = 488 nm, emission filter = 520 (50) nm.

Image Processing. All NIR and GFP fluorescence images were restored using fifty iterations of the CMLE method in Huygens Professional deconvolution software (15.10). DIC images were corrected by flat-field correction to compensate for uneven illumination. A background image (i2) was created by applying a 50 pixel median filter to the source image (i1). Using the Calculator Plus plugin in ImageJ the "Divide" function was used, corrected image = (i_1/i_2) x $(k_1 + k_2)$, where k1= I_{flu} of (i1) and k2= 0. Time-lapse mean intensity was calculated using the measure function in ImageJ.

Surface analysis of images. The area and volume of cellular fluorescence was measured using the Surface tool in Imaris image processing software (v7.2.4, Bitplane Scientific). The parameters for the Surface visualization algorithm were selected based on a ROI, then applied to the entire dataset as a way to reduce processing time. The specified grey level range representing the fluorescence of **1** was manually selected using an absolute intensity threshold. Background subtraction and smoothing was performed using a Gaussian filter 0.127 µm. The resulting graphical interpretation of the detected Surface was modified by a grain size of 0.254 µm, and presented as an "iso-surface".

Supplemental Information

Supporting movies 1-9, and supporting figures 1-4 and can be found with this article online at…

Authors Contributions

D.O.S. conceived and directed the research. P.G. provided prodigiosin and supervised the synthetic liposomal model experiments which were carried out by N.B. S.C. and M.M. carried out the imaging experiments. D.W. and H.C.D. carried out the synthesis of **1**. J.C.S. provided HeLa-LAMP1 cells. D.S. assisted with and advised on imaging experiments. D.O.S. and S.C. wrote the manuscript with all authors contributing to the final version.

Competing financial interests

DOS declare the following competing financial interest. A patent application has been filed on azadipyrromethene based NIR fluorophores (PCT/EP2010/065991) in which he has a financial interest.

References and Notes

1. van Meer, G., Voelker, D.R., Feigenson, G.W. (2008). Membrane lipids: where they are and how they behave. *Nat. Rev. Mol. Cell Biol. 9*, 112-124.

2. Casey, J. R., Grinstein, S., Orlowski, J. (2010). Sensors and regulators of intracellular pH. *Nat. Rev. Mol. Cell. Biol. 11*, 50-61.

3. Xu, H., Ren, D. (2015). Lysosomal Physiology. *Annu. Rev. Physiol. 77*, 57-80.

4. Xiong, J., Zhu, M. X. (2016). Regulation of lysosomal ion homeostasis by channels and transporters. *Sci. China Life Sci. 59*, 777-791.

5. Graves, A. R., Curran, P. K., Smith, C. L., Mindell, J. A. (2008). The Cl^-/H^+ antiporter ClC-7 is the primary chloride permeation pathway in lysosomes. *Nature. 453*, 788-792.

6. Hosogi, S., Kusuzaki, K., Inui, T., Wang, X., Marunaka, Y. (2014). Cytosolic chloride ion is a key factor in lysosomal acidification and function of autophagy in human gastric cancer cell. *J. Cell. Mol. Med. 18*, 1124-1133.

7. Busschaert, N., Gale, P.A. (2013). Small-molecule lipid-bilayer anion transporters for biological applications. *Angew. Chem. Int. Ed. 52*, 1374-82.

8. Aits, S., Jäättelä, M. (2013). Lysosomal cell death at a glance. *J. Cell Sci. 126*, 1905-12.

9. (a) Busschaert, N., Park, S.H., Baek, K-H., Choi, Y.P., Park, J., Howe, E.N.W., Hiscock, J.R., Karagiannidis, L.E., Marques, I., Félix, V., Namkung, W., Sessler, J.L., Gale, P.A., Shin I. (2017). A synthetic ion transporter that disrupts autophagy and induces apoptosis by perturbing cellular chloride concentrations. *Nat. Chem. 9*, 667-675. (b) Rodilla, A.M., Korrodi-Gregorio, L., Hernando, E., Manuel-Manresa, P., Quesada, R., Perez-Tomas, R., Soto-Cerrato, V. (2017). Synthetic tambjamine analogues induce mitochondrial swelling and lysosomal dysfunction leading to autophagy blockade and necrotic cell death in lung cancer. *Biochem. Pharm. 126*, 23-33.

10. Ko, S.-K., Kim, S. K., Share, A., Lynch, V.M., Park, J., Namkung, W., Van Rossom, W., Busschaert, N., Gale, P. A., Sessler, J. L., Shin, I. (2014). Synthetic ion transporters can induce apoptosis by facilitating chloride anion transport into cells. *Nat. Chem. 6*, 885-892.

11. Soto-Cerrato, V., Manuel-Manresa, P., Hernando, E., Calabuig-Farinas, S., Martinez-Romero, A., Fernández-Duenas, V., Sahlholm, K., Knopfel, T., Garcia-Valverde, Maria., Rodilla, A.M., Jantus-Lewintre, E., Farraas, R., Ciruela, F., Perez-Tomas, Ricardo., Quesada, R. (2015). Facilitated anion transport induces hyperpolarization of the cell membrane that triggers differentiation and cell death in cancer stem cells. *J. Am. Chem. Soc. 137*, 15892-15898.

12. Darshan, N., Manonmani, H.K. (2015). Prodigiosin and its potential applications. *J. Food Sci. Technol. 52*, 5393-5407.

13. Johansson, A. C., Appelqvist, H., Nilsson, C., Kågedal, K., Roberg, K., Öllinger, K. (2010). Regulation of apoptosis-associated lysosomal membrane permeabilization. *Apoptosis 15*, 527-540.

14. Matsuyama, S., Llopis, J., Deveraux, Q. L., Tsien, R. Y., Reed, J. C. (2000). Changes in intra-mitochondrial and cytosolic pH: early events that modulate caspase activation during apoptosis. *Nat. Cell Biol. 2*, 318-25.

15. Hu, D. X., Withall, D. M., Challis, G. L., Thomson, R. J. (2016). Structure, chemical synthesis and biosynthesis of prodiginine natural products. *Chem. Rev. 116*, 7818-7853.

16. Williamson, N. R., Fineran, P. C., Gristwood, T., Chawrai, S. R., Leeper, F. J., Salmond, G. P. C. (2007). Anticancer and immunosuppressive properties of bacterial prodiginines. *Future Microbiol. 2*, 605-618.

17. Sessler, J. L., Eller, L. R., Cho, W.-S., Nicolaou, S., Aguilar, A., Lee, J. T., Lynch, V. M., Magda, D. J. (2005). Synthesis, anion-binding properties, and in vitro anticancer activity of prodigiosin analogues. *Angew. Chem. Int. Ed. 117*, 6143-6146.

18. Seganish, J. L., Davis, J. T. (2005). Prodigiosin is a chloride carrier that can function as an anion exchanger. *Chem. Commun*. **46**, 5781-5783.

19. Ohkuma, S., Sato, T., Okamoto, M., Matsuya, H., Arai, K., Kataoka, T.,Wasserman, H. H. (1998). Prodigiosins uncouple lysosomal vacuolar-type ATPase through promotion of H^+/Cl^- symport. *Biochem. J. 741*, 731-741.

20. Kataoka, T., Muroi, M., Ohkuma, S., Waritani, T., Magae, J., Takatsuki, A., Takatsukie, A., Kondo, S., Yamasaki, M., Nagai, K. (1995). Prodigiosin 25-C uncouples vacuolar type H^+-ATPase, inhibits vacuolar acidification and affects glycoprotein processing. *FEBS Lett. 359*, 53-59.

21. Gale, P. A. (2011). From anion receptors to transporters. *Acc. Chem. Res. 44*, 216-226.

22. Davis, J. T., Okunola, O. (2010). Recent advances in the transmembrane transport of anions. *Chem. Soc. Rev. 39*, 3843-3862.

23. Data available on the Internet at https://dtp.cancer.gov/dtpstandard/dwindex/index.jsp and the NSC number for prodigiosin is 47147.

24. Goard, C. A., Schimmer, A. D. (2013). An evidence-based review of obatoclax mesylate in the treatment of hematological malignancies. *Core Evidence*. *8*, 15-26.

25. Sato, T., Konno, H., Tanaka, Y., Kataoka, T., Nagai, K., Wasserman, H.H. Ohkuma, S. (1998). Prodigiosins as a new group of H^+/Cl^- symporters that uncouple proton translocators. *J. Biol. Chem. 273*, 21455-21462.

26. Castillo-Avila, W. Abal, M., Robine, S., Perez-Tomas, R. (2005). Non-apoptotic concentrations of prodigiosin (H^+/Cl^- symporter) inhibit the acidification of lysosomes and induce cell cycle blockage in colon cancer cells. *Life Sci. 78*, 121-127.

27. Francisco, R., Pérez-Tomás, R., Gimènez-Bonafé, P., Soto-Cerrato, V., Giménez-Xavier, P., Ambrosio, S. (2007). Mechanisms of prodigiosin cytotoxicity in human neuroblastoma cell lines. *Eur. J. Pharmacol. 572*, 111-119.

28. Díaz de Greñu, B., Iglesias Hernández, P., Espona, M., Quiñonero, D., Light, M. E., Torroba, T., Perez-Tomas, R., Quesada, R. (2011). Synthetic prodiginine obatoclax (GX15-070) and related analogues: anion binding, transmembrane transport, and cytotoxicity properties. *Chem. Eur. J. 17*, 14074-83.

29. Nakashima, T., Tamura, T., Kurachi, M., Yamaguchi, K., Oda, T. (2005). Apoptosis-mediated cytotoxicity of prodigiosin-like red pigment produced by γ-*proteobacterium* and its multiple bioactivities. *Biol. Pharm. Bull. 28*, 2289-2295.

30. Hornick, J.R., Vangveravong, S., Spitzer, D., Abate, C., Berardi, F., Goedegebuure, P., Mach, R.H., Hawkins, W.G. (2012). Lysosomal membrane permeabilization is an early event in sigma-2 receptor ligand mediated cell death in pancreatic cancer. *J. Exper. Clin. Cancer Res. 31*, 41.

31. Han, J., Burgess, K. (2010). Fluorescent indicators for intracellular pH. *Chem. Rev. 110*, 2709-2728.

32. Pierzyńska-Mach, A., Janowski, P.A., Dobrucki, J.W. (2014). Evaluation of acridine orange, lysotracker red, and quinacrine as fluorescent probes for long-term tracking of acidic vesicles. *Cytometry A, 85A*, 729-737.

33. Petersen, N.H.T., Kirkegaard, T., Jäättelä, M. (2014). Lysosomal Stability Assay. *Bio-protocol, 4*, e1162.

34. Grossi, M., Morgunova, M., Cheung, S., Dimitri Scholz, D., Conroy, E., Terrile, M., Panarella, A., Simpson, J.C., Gallagher, W.M., O'Shea, D.F. (2016). Lysosome triggered near infra-red fluorescence; imaging of cellular trafficking processes in real-time. *Nat. Commun. 7*, 10855.

35. Ge Y., O'Shea, D.F. (2016). Azadipyrromethenes: from traditional dye chemistry to leading edge applications. *Chem. Soc. Rev. 45*, 3846-3864.

36. Tafani, M., Cohn, J.A., Karpinich, N.O., Rothman, R.J., Russo, M.A., Farber, J.L. (2002). Regulation of intracellular pH mediates Bax activation in HeLa cells treated with staurosporine or tumour necrosis factor-α. *J. Biol. Chem. 277*, 49569-49576.

37. Busschaert, N., Kirby, I. L., Young, S., Coles, S. J., Horton, P. N., Light, M. E., Gale, P. A. (2012). Squaramides as potent transmembrane anion transporters. *Angew. Chem. Int. Ed. 51*, 4426-4430.

38. Davis, J.T. (2010). *Topics in Heterocyclic Chemistry*, eds. Gale, P. A. and Dehaen, W. Springer, New York, *24*, 145-176.

39. Marcus, Y. (1991). Thermodynamics of solvation of ions part 5 – Gibbs free energy of hydration at 298.15 K. *J. Chem. Soc. Faraday Trans.*, *87*, 2995-2999.

40. Wu, X., Judd, L.W., Howe, E.N.H., Withecombe, A.M., Soto-Cerrato, V., Li, H., Busschaert, N., Valkenier, H., Pérez-Tomás, R., Sheppard, D.N., Jiang, Y.-B., Davis, A.P., Gale, P.A. (2016). Nonprotonophoric electrogenic Cl⁻ transport mediated by valinomycin-like carriers. *Chem*. *1*, 127-146.

41. Kilpatrick, B. S., Eden, E. R., Hockey, L. N., Futter, C. E., Patel, S. (2015). Methods for monitoring lysosomal morphology. *Methods Cell Biol*. *126*, 1-19.

42. Panarella, A., Bexiga, M. G., Galea, G., Neill, E. D. O. Salvait, A., Dawson, K.A., Simpson, J.C. (2016). A systematic high-content screening microscopy approach reveals key roles for Rab33b, OATL1 and Myo6 in nanoparticle trafficking in HeLa cells. *Sci. Rep*. *6*, 1-11.
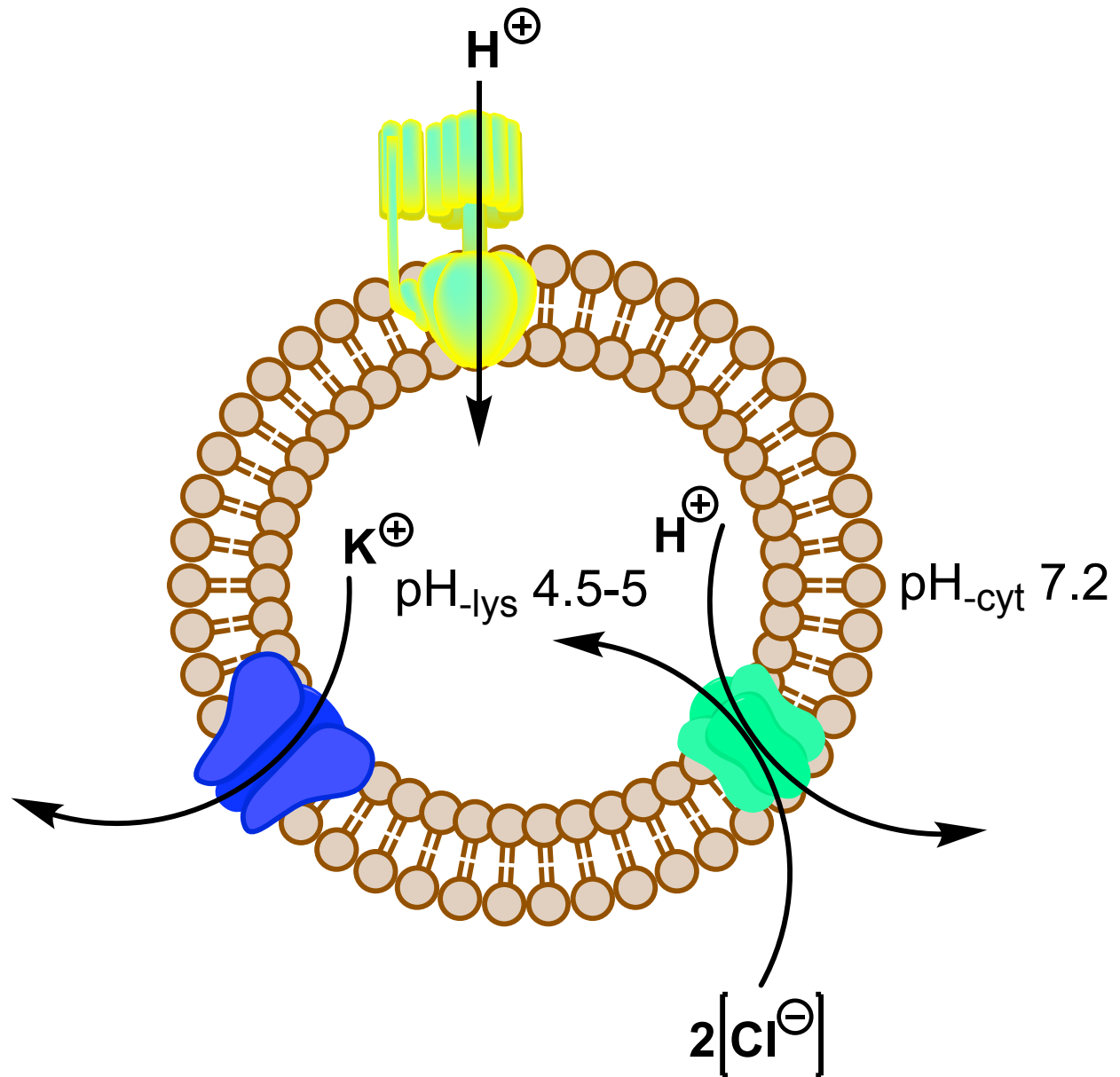
Figure 1. Lysosomal ion transport

V-type ATPase proteins (yellow) pump protons into the lysosome, decreasing pH-$_{lys}$ with the positive membrane potential dissipated by the efflux of potassium ions (K^+) through cation channels (blue) and influx of chloride ions (Cl^-) through ClC-7 (green) anion channels.
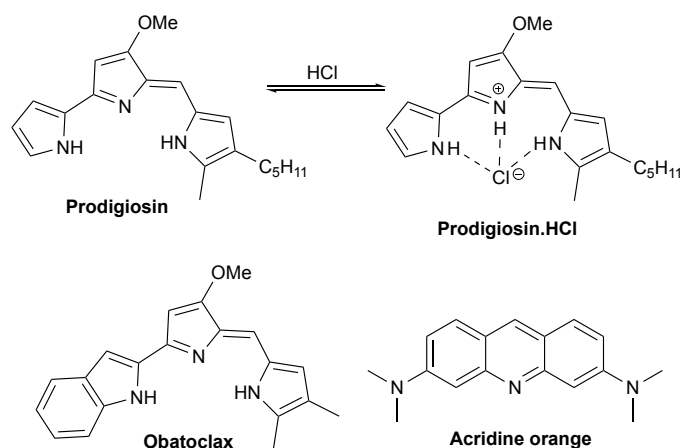
Figure 2. Structure of prodigiosin, its HCl bound ion pair, obatoclax and acridine orange
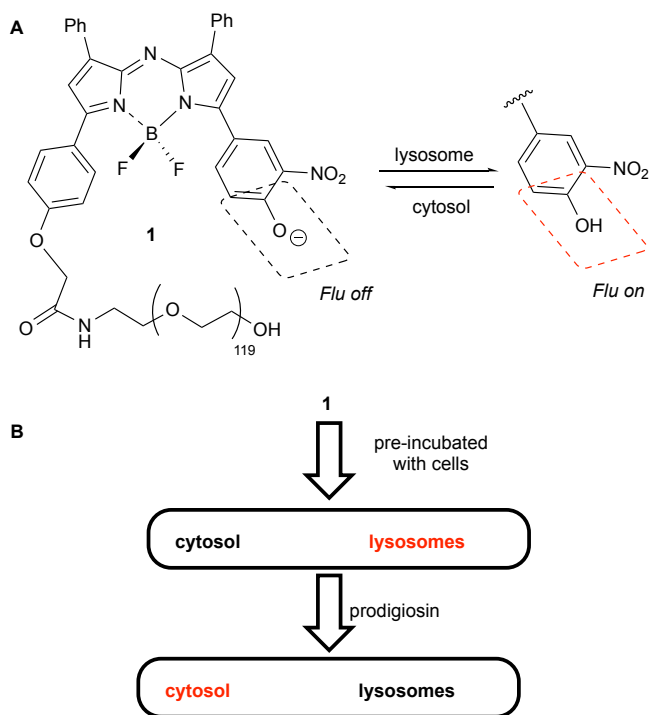

Figure 3. Structure of lysosomal responsive NIR-AZA probe 1 used and goals of this study (A) NIR-emission from **1** is quenched as phenolate (grey box) and turned on when protonated as its phenol (red box). (B) Goal for real-time fluorescence imaging of cellular responses to prodigiosin. Black color = non-emissive; red color = NIR-emissive).
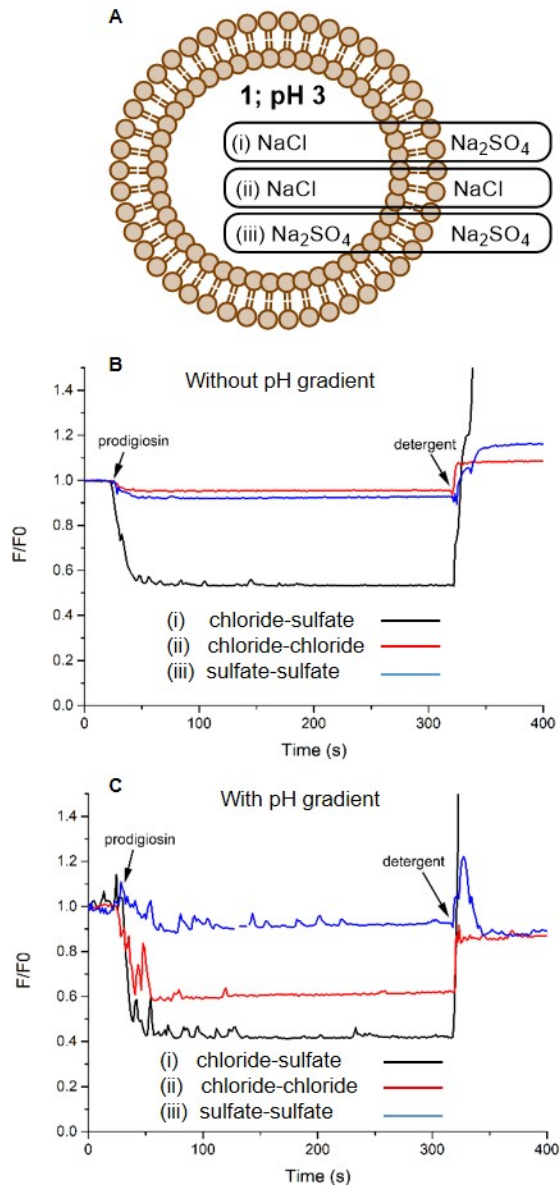
Figure 4. Confirmation of H$^+$/Cl$^-$ symport by prodigiosin (0.1 mol% w.r.t. lipid) using responsive probe **1** (135 µM)

(A) Experiments performed with **1** utilizing synthetic POPC:cholesterol unilamellar vesicles with (i) intra-vesicular salt NaCl (489 mM) and extra-vesicular salt Na$_2$SO$_4$ (162 mM); (ii) intra-vesicular salt NaCl (489 mM) and extra-vesicular salt NaCl (489 mM); (iii) intra-vesicular salt Na$_2$SO$_4$ (162 mM) and extra-vesicular salt Na$_2$SO$_4$ (162 mM). (B) Graphs showing prodigiosin induced changes in F/F$_0$ for **1** at 720 nm without an applied pH gradient. (C) Graphs showing prodigiosin induced changes in F/F$_0$ for **1** at 720 nm with an applied pH gradient. Each graph represents the average of three experiments.
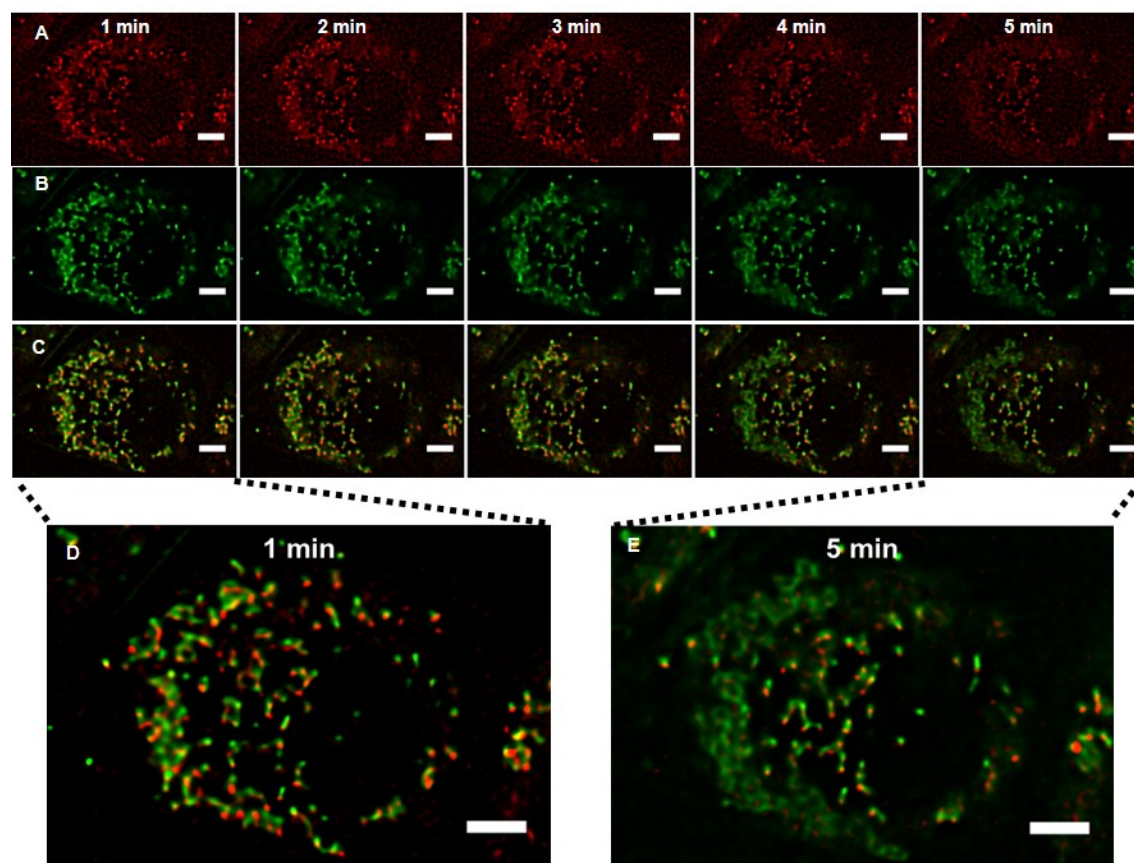
Figure 5. Five min time-lapse of changes in NIR emission from **1** (10 µM; red color) and GFP (green color) in HeLa-LAMP1/GFP cells following treatment with prodigiosin (50 µM). (A) Individual time points of emission from **1** following treatment with prodigiosin, for movie see Movie S1; (B) Individual time points of GFP emission following treatment with prodigiosin, for the movie see Movie S2; (C) Individual time points showing overlaid images of NIR and GFP emissions following treatment with prodigiosin, for the movie see Movie S3. (D), (E) Enlarged view at 1 min and 5 min post treatment with prodigiosin. Scale bars = 5 µm. For full field of view including the cell shown in this figure see Figure S2 and Movie S4.
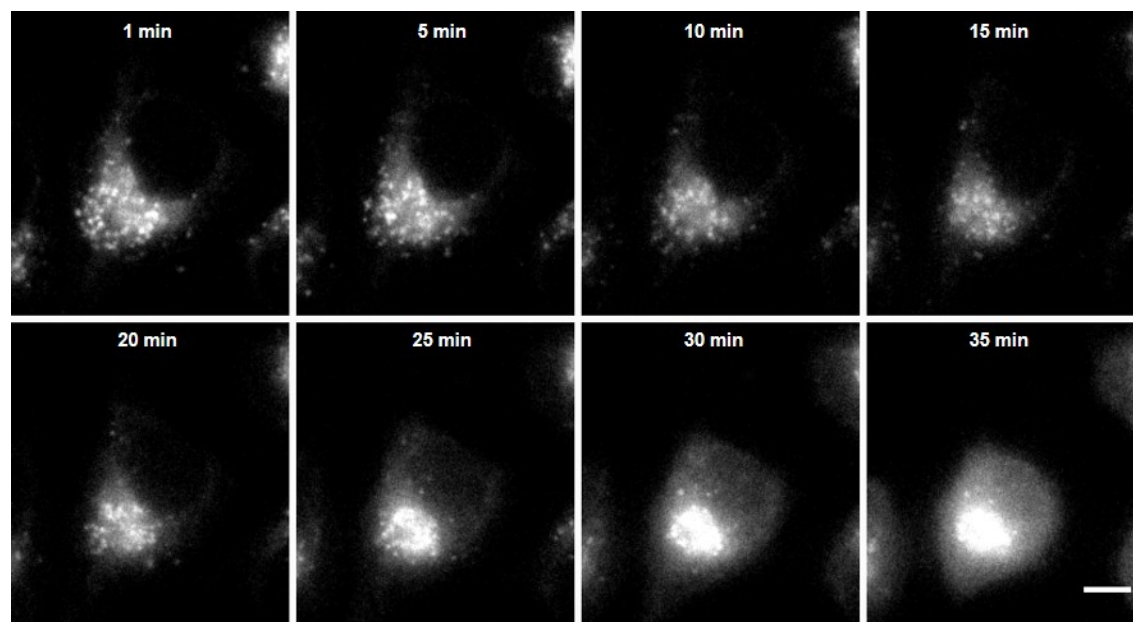
Figure 6. Continuous widefield imaging of the effects on HeLa Kyoto cells (pre-incubated with 1 for 2 hr) for 40 min following treatment with prodigiosin (Movie S5). NIR emission from **1** shown in white for clarity; conc **1** = 10 µM, prodigiosin = 50 µM; scale bar = 20 µm.
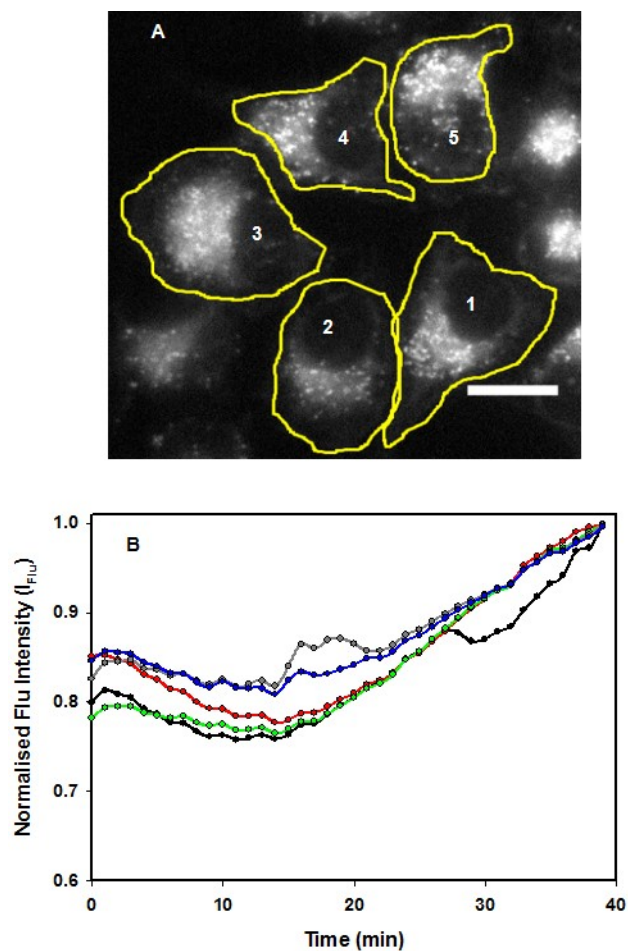
Figure 7. Changes in intracellular fluorescence intensity from probe 1 (10 µM) in HeLa Kyoto cells over a 40 min time period post prodigiosin (50 µM) treatment. Widefield microscope images taken in a single focal plane with NIR emission from **1** shown in white for clarity.

(A) Five cells selected as ROIs (yellow traces) of which their mean fluorescence intensity was measured every 20 sec for 40 min, scale bar = 40 µm, (Movie S6). (B) Normalized fluorescence intensity from each cellular ROI plotted versus time. Cells: 1 (blue trace); 2 (grey trace); 3 (green trace); 4 (black trace); 5 (red trace).
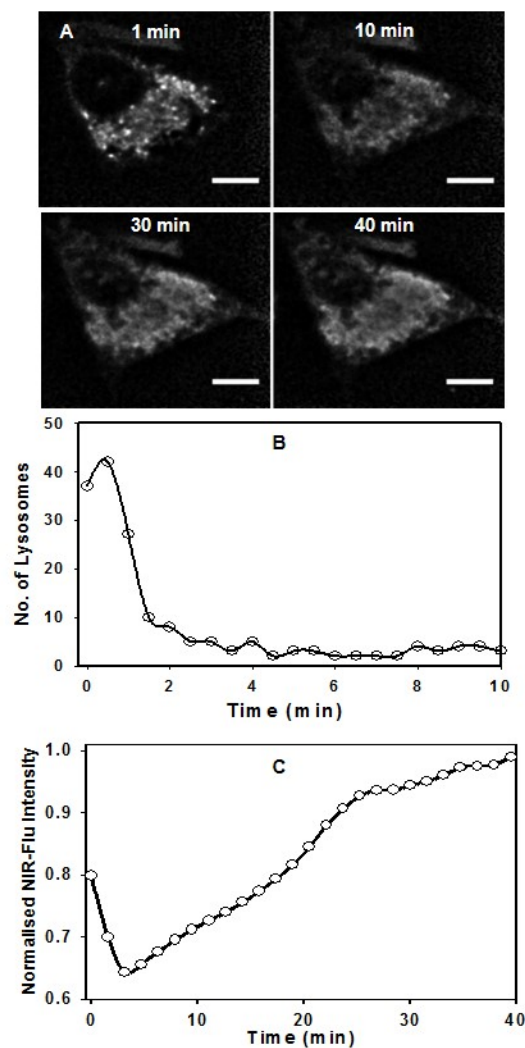
Figure 8. 4D Continuous NIR-fluorescence imaging of HeLa Kyoto cells response to prodigiosin utilizing probe **1**, for movie see Movie S7.

(A) Widefield live-cell images acquired after 1, 10, 20, 30 and 40 min post-treatment with prodigiosin. NIR emission from **1** shown in white for clarity, scale bar = 20 μm. (B) Plot showing the changes in number of NIR fluorescent lysosomes from 1 to 10 min post prodigiosin treatment. (C) Plot showing changes in cellular NIR-emission intensity (I_{flu}) over a 40 min time period post prodigiosin treatment.
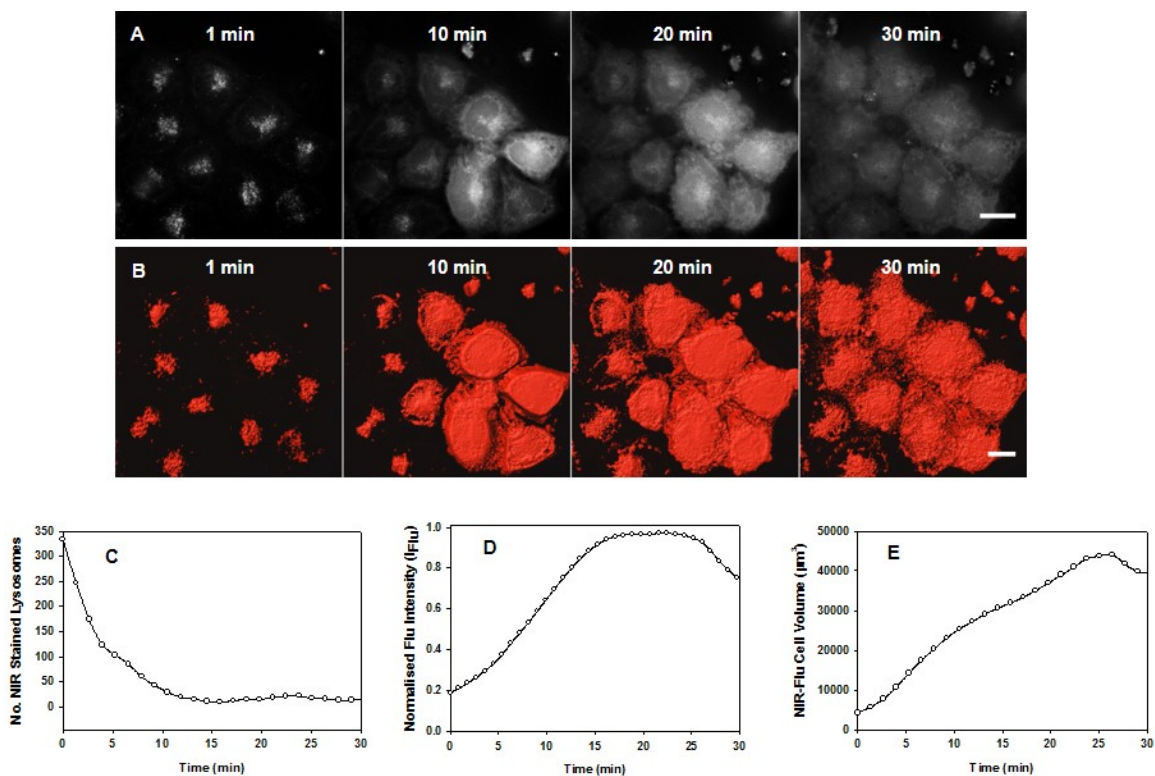
Figure 9. 4D Continuous widefield imaging of **1** in HeLa Kyoto cells responding to prodigiosin (100 μM) over a 30 min time period.

(A) Representative individual time point fluorescence images at 1, 10, 20 and 30 min, NIR emission from **1** shown in white for clarity (Movie S8). (B) Graphic illustration of the increasing cellular volume having an NIR-emission from **1** over time (Movie S9). (C) Changes in the number of fluorescent lysosomes over time from within the entire field of view. (D) Normalized fluorescence intensity plotted versus time for the entire field of view. (E) Plot of the increasing fluorescent cellular volume versus time of the entire field of view. Scale bars = 20 μm.